INTERNATIONAL SOCIETY FOR SOIL MECHANICS AND GEOTECHNICAL ENGINEERING



This paper was downloaded from the Online Library of the International Society for Soil Mechanics and Geotechnical Engineering (ISSMGE). The library is available here:

https://www.issmge.org/publications/online-library

This is an open-access database that archives thousands of papers published under the Auspices of the ISSMGE and maintained by the Innovation and Development Committee of ISSMGE.

Constitutive model for large load reversals and stress rotation in soils Modèle rhéologique des grandes décharges et rotation des contraintes dans les sols

C.T.Christensen – Danish Geotechnical Institute, Lyngby, Denmark
R.B.Nelson – Department of Civil Engineering, University of California, Los Angeles, Calif., USA

ABSTRACT: A time independent constitutive model with an inherent capability for capturing both elastic and inelastic effects of large load reversals and stress field rotations in soils has been developed. The model makes full use of 'sublayer information' as originally proposed for nested surfaces type of models. The sublayer information is introduced through 'friction stress' tensors as state variables. A mechanical analogy provides a straightforward and rational basis for the evolution of the state variables. The model is calibrated to a series of triaxial tests and is shown to successfully extrapolate to complex stress paths as applied in torsion-shear tests with large load reversals and stress field rotation. An ABAQUS user material subroutine employing so called 'compatibility iterations' has been developed and verified. A friction mechanism with smooth stress-strain behavior is suggested as a way of smoothing the model response.

RESUME: Un modèle rhéologique indépendent du temps capable de prendre en compte le comportement élastique et inélastique lors des grandes décharges et rotation des contraintes dans les sols est développé. Le modèle utilise le principe de l'information de la subcouche proposé à l'origine pour les modèles du type surfaces réticulées. Ce principe est introduit par l'intermédiaire des paramètres d'état donnés par les tenseurs "contraintes des frottement". Une analogie mécanique fournit une base directe et rationelle pour l'évolution de ces paramètres d'état. Le modèle est étalonné sur des essais triaxiaux et extrapolé avec succès à des sollicitations complexes comme celles de cisaillement par torsion avec des décharges de grandes amplitudes et des rotations du champ des contraintes. Un sous-programme d'ABAQUS utilisant "les itérations de compatibilité" est développé et vérifié. Un mécanisme de frottement dépendant du comportement contrainte-déformation est proposé pour lisser la réponse du modèle.

1. INTRODUCTION

A 3-D constitutive model for soils has been developed on the basis of the mechanical behavior of a serial assembly of an element for non-linear elasticity, an element for pressure-volume plasticity and a series of friction-slip mechanisms for inelastic and recoverable shear effects, see figure 1, derived from Christensen (1995). The first two elements have been gathered in the left model part, named PR, while all friction slip mechanisms (here 4) have been gathered in the right model part, named SH.

The model can be categorised as belonging to the family of nested surfaces models, as originally and individually proposed by Mróz (1967) and Iwan (1967).

Compared to most all nested surfaces models, the new constitutive model presented here stays true to the original idea of Iwan of employing a series of friction mechanisms, interpretable as sublayers of the material. Compared to the models by Mróz (1978-1983) and Prévost (1977, 1978), the new model does not integrate the effect of all friction mechanisms into an overall plastic modulus and it has no plasticity hierarchy dictating in which order plasticity (or shear slip) can develop or be active. Rather the new model keeps record of a parallel stress

tensor split within each of k = 1..N friction-slip mechanisms (sublayers):

$$\sigma_{ij} = \sigma_{ij}^{friction(k)} + s_{ij}^{excess(k)}; \quad k = 1..N$$
 (1)

For each friction mechanism the friction stress tensor will be stored as an internal tensor state variable and the deviatoric excess stress tensor can be considered a 'back-stress' from the actual stress state. Excess stresses are defined deviatoric because this definition has proven optimal for data matching.

In treating the friction mechanisms as individual components and keeping record of the friction stresses in each mechanism, the new model makes full use of sublayer information, otherwise partly lost when the combined effect of all mechanisms are integrated into one plastic hardening modulus.

Model strain increments are the sum of individual contributions:

$$d\varepsilon_{ij} = d\varepsilon_{ij}^{EL} + \frac{d\varepsilon_{vol}^{PL}}{3} \delta_{ij} + \frac{1}{N} \sum_{k=1}^{N} \left(d\varepsilon_{ij}^{friction(k)} + d\varepsilon_{ij}^{excess(k)} \right)$$
 (2)

where EL and PL mean elastic and plastic, respectively, and N is the number of friction mechanisms in the model.

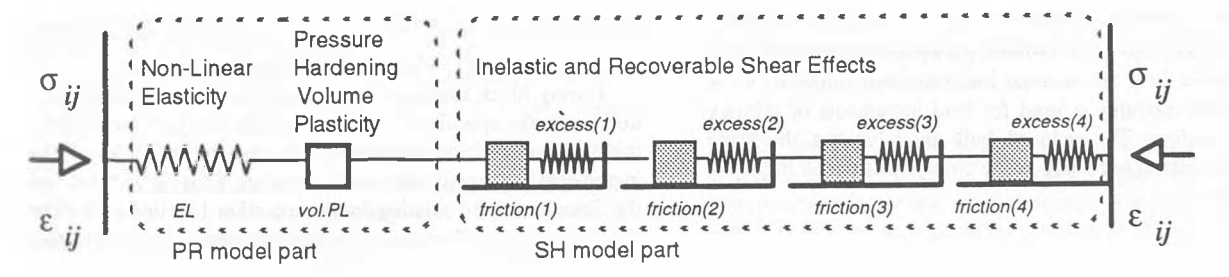


Figure 1 Mechanical assembly of constitutive model with N = 4 friction mechanisms

2. MODEL PART, PR

2.1 Non-linear elasticity

The non-linear elastic model makes use of bulk and shear moduli, K and G, which are functions of the first invariant of stress and the squareroot of the second invariant of deviatoric stress, respectively:

$$K = K(I_1); \qquad G = G(J) \tag{3}$$

$$I_1 = \sigma_{11} + \sigma_{22} + \sigma_{33} \tag{4}$$

$$J = \sqrt{J_2'} = \sqrt{\frac{1}{2} s_{ij} s_{ji}}$$

$$= \sqrt{\left(s_{11}^2 + s_{22}^2 + s_{33}^2\right) / 2 + s_{12} s_{21} + s_{13} s_{31} + s_{23} s_{32}}$$
(5)

where the deviatoric stress tensor components as usual are defined from:

$$s_{ij} = \sigma_{ij} - \frac{I_1}{3} \delta_{ij} \tag{6}$$

An isotropic non-linear hyperelastic law can be established on the basis of the I_1 dependent K and the I_2 dependent G:

$$\varepsilon_{\ddot{y}}^{EL} = \frac{I_1}{3K} \frac{\delta_{\ddot{y}}}{3} + \frac{s_{\ddot{y}}}{2G} \tag{7}$$

Differentiation of this law provides the rate form:

$$d\varepsilon_{\bar{g}}^{EL} = S_{\bar{g}\,kl} d\sigma_{kl} \tag{8}$$

where

$$S_{ijkl} = \frac{\partial \varepsilon_{ij}^{EL}}{\partial \sigma_{kl}}$$

$$= \frac{\delta_{ij} \delta_{kl}}{9K} \left(1 - \frac{1}{K} \frac{dK}{dl_1} I_1 \right)$$

$$+ \frac{1}{2G} \left(\left(-\frac{1}{G} \right) \frac{dG}{dJ} \frac{s_{kl}}{2J} s_{ij} + \left(\delta_{ik} \delta_{jl} - \frac{\delta_{ij} \delta_{kl}}{3} \right) \right)$$
(9)

The stiffness rate form may finally be found inverting the Jacobian flexibility matrix [S].

2.2 Pressure-volume plasticity

Pressure plasticity is added to the PR model part by memorizing as an internal state variable the maximum pressure ($p = \text{mean stress} = I_1/3$) the material has ever been subjected to. A reduced bulk modulus is used for load increments of primary pressure loading. The reduced bulk modulus has the same functional stress dependency as the purely elastic bulk modulus, only softer.

3. MODEL PART, SH

Inelastic and partly recoverable shear effects are taken care of by the friction-slip mechanisms of the SH model part. The parallel stress tensor split, (1), and its updating for a load increment, is very important as it defines the evolution of the friction stress tensors, i.e. the internal state variables for kinematic hardening.

The evolution will be understood from a study of the behavior of a single friction mechanism (seen from vertical above), loaded by a 2-D $\{P\}$ vector, and held in place by friction reaction against the base, $\{F\}$, and two spring reactions, the resultant of which forms the 'excess' vector $\{S\}$, where brackets $\{\}$ denote a vector.

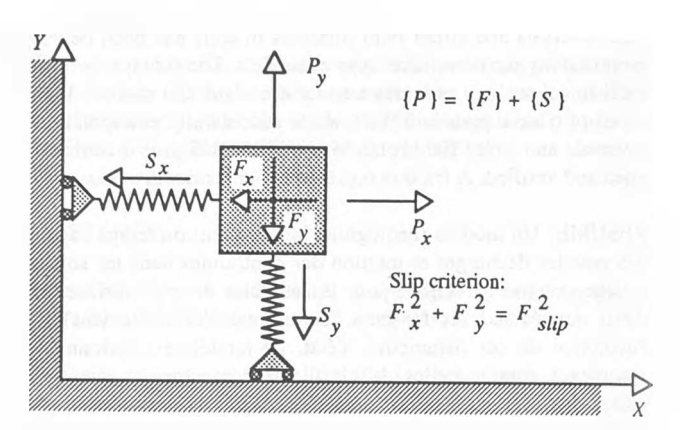


Figure 2 Split of applied 2-D load, {P}, into reactions of base friction, {F}, and excess, {S}

In figure 2, a friction box is assumed to rest on a horizontal frictional base (the X-Y plane) and to be held in place by base friction and two horizontal supporting springs. Like the friction mechanisms in the constitutive model, the friction block will not respond to loading as long as the friction against the base can resist the applied loading. However, once the frictional slip capacity of the block is exhausted, any additional loading will produce movement. For the sake of illustration, consider a simple circular friction slip criterion of the form:

$$||F|| = \sqrt{F_x^2 + F_y^2} = F_{slip}$$
 (10)

If the friction block is loaded to friction slip capacity, and the applied load, $\{P\}$, is increased further, then the block will move, causing the transfer of excess loading to the supporting springs. Hereafter, the load is carried in parallel as the sum of a base friction reaction and an excess spring reaction. An interesting study of the evolution of friction and excess reactions for various applied load paths can then be made.

Given the existing split of the applied load, $\{P\}$, into friction and excess reactions, $\{F\}$ and $\{S\}$, the problem is to determine the new split, $\{F_{new}\}$ and $\{S_{new}\}$, for an updated load, $\{P_{new}\} = \{P\} + \{dP\}$, where $\{dP\}$ is a load increment.

During block movement, the direction of the friction reaction is always opposite to the direction of the movement. Also, the direction of block movement defines the direction of the incremental change in the excess reaction, $\{dS\}$. It follows that the direction of the existing friction reaction $\{F\}$ in fact defines the direction of differential change in the excess reaction, $\{dS\}$,

and they are consequently proportional, with an unknown proportionality constant $d\lambda$:

$$\{dS\} = d\lambda \{F\} \tag{11}$$

From this observation, the equilibrium equations and the slip criterion can be used to solve for $\{F_{new}\}$ and $d\lambda$:

$$\begin{aligned}
\{F_{new}\} &= \{P_{new}\} - \{S_{new}\} \\
&= \{P\} + \{dP\} - \{S\} - \{dS\} \\
&= (\{P\} - \{S\}) + \{dP\} - \{dS\} \\
&= \{F\} + \{dP\} - d\lambda \{F\}
\end{aligned} \tag{12}$$

$$||F_{new}|| - F_{slip} = 0 ag{13}$$

A projection rule for the determination of the updated split of the applied load, following a load increment, appears as follows, directly following the algebra of the above two equations.

- Take the existing friction, {F} = {P}-{S}, and add the load increment, {dP}, to get {F}+{dP}.
- 2. Project the point $\{F\}+\{dP\}$ in the direction of $-\{F\}$ until intersection with the slip criterion surface. The intersection is the updated friction reaction, $\{F_{new}\}$.
- 3. Finally: $\{S_{new}\} = \{P\} + \{dP\} \{F_{new}\}$

The projection rule is illustrated in figure 3.

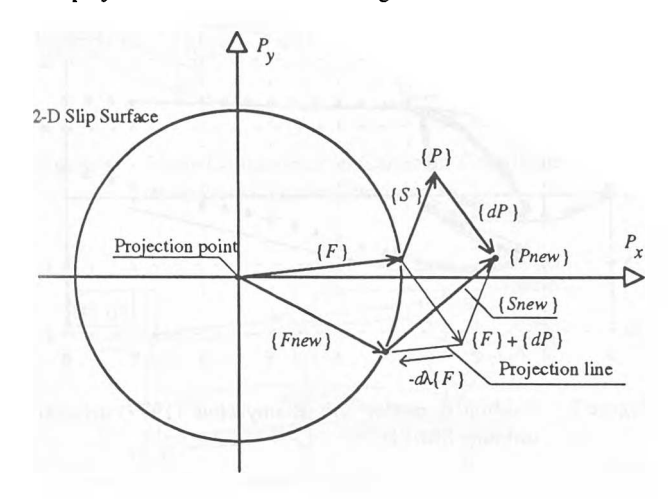


Figure 3. Projection rule for updating load split

An interesting study of the load split under 360 degree pure rotation of the load $\{P\}$, with maintained magnitude, is illustrated in figure 4. Initially the block has been loaded to $\{P\}$ = $\{2,0\}$ causing $\{F\}$ = $\{1,0\}$ and $\{S\}$ = $\{1,0\}$. Using the projection rule, the load split is updated in 50 subsequent incremental steps of 360 degree rotation of $\{P\}$. The initial and final $\{S\}$ are shown in heavy lines in figure 4.

In a generalisation into tensorial stress space, vector $\{F\}$ becomes the 6×1 deviatoric vector $\{\sigma^{friction}\}$ - $\{p\}$, where $\{p\}^T = \{p \mid p \mid p \mid 0 \mid 0 \mid 0\}$ is the pressure tensor, and vector $\{S\}$ becomes the 6×1 excess deviatoric stress, $\{s\}$. The generalised projection rule for updating the friction stress in mechanism number k becomes:

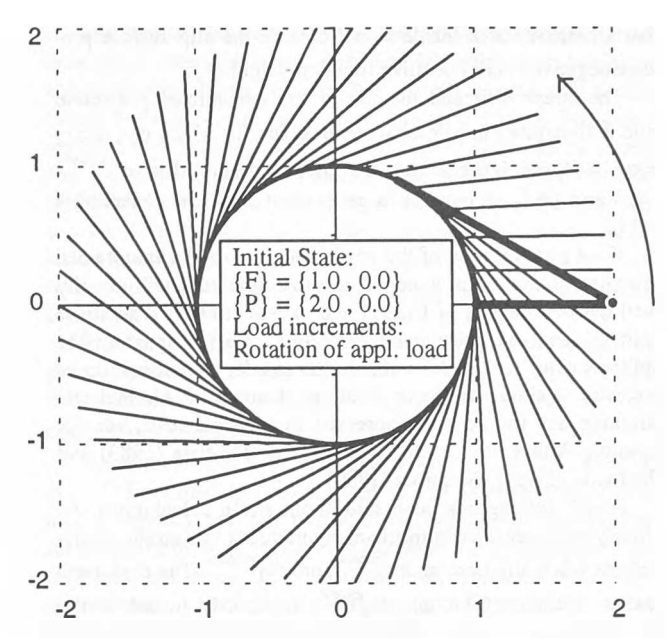


Figure 4. Updated load splits under rotation of load, {P}

where f_k is the shear slip function for friction mechanism k and brackets {} now symbolise 6×1 matrix vectors, e.g. transposed $\{\sigma\}^T = \{\sigma_{11} \ \sigma_{22} \ \sigma_{33} \ \sigma_{12} \ \sigma_{13} \ \sigma_{23}\}.$

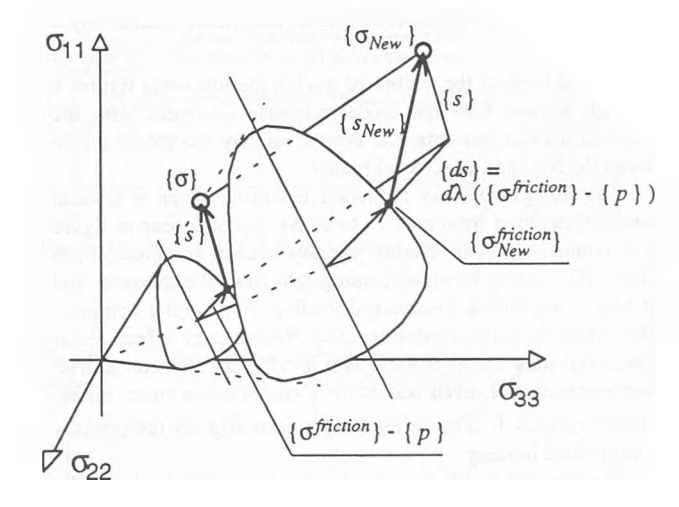


Figure 5. Generalised projection rule, for updating of friction mechanism stress split

The shear slip function, f_k , is expressed in terms of stress invariants of friction stress, not entire stress, and it defines a near conical slip surface with a rounded triangular cross section. It is devised as a potential function of friction stress such

that all stress states inside / on / outside the slip surface produce negative / zero / positive function values of f_k .

The stress split and the use of the generalized projection rule is illustrated in principal stress space (in which $\sigma_{12} = \sigma_{13} = \sigma_{23} = 0$), see figure 5. Note the important point that $\{\sigma^{friction}\}$ - $\{p\}$ and $\{ds\}$ are parallel (a generalisation of the observation (11)).

For a pure rotation of the stress state, i.e. under maintained principal stresses, the generalized projection rule will equally well define rotations of friction and excess stresses. The stress split (1) and the generalized projection rule for updating the split provides the model with the means for determination of inelastic straining for pure rotation of stress. Such inelastic straining has indeed been observed in physical tests, see for example Arthur et al. (1980), Ishihara & Towhata (1983) and Pradel, Ishihara & Gutierrez (1990).

So far nothing has been said about strain calculations. As already mentioned, each mechanism produces two strain contributions when slip occurs, de_{ij}^{excess} and $de_{ij}^{friction}$. The deviatoric excess strain contribution, de_{ij}^{excess} , is directly linked to the deviatoric excess stress, ds_{ij}^{excess} , through a Young's modulus and Poisson's ratio, v = 0.5, one set for each mechanism. The friction strain contribution, $de_{ij}^{friction}$, is given the same magnitude (or tensor norm) as ds_{ij}^{excess} , however with a different orientation according to the gradient of a plastic (or rather 'slip') potential function, again, evaluated at the friction stress.

4. MODEL CALIBRATION USING CONVENTIONAL TESTS

A model with 4 friction mechanisms, see figure 1, was calibrated using data from three conventional triaxial tests, taken from Boonyachut (1977), and one isotropic compression test, taken from Prabucki & Lade (1990). All tests used the same loose (initial void ratio, e = 0.81) Santa Monica Beach sand. The triaxial tests were carried out under constant confining pressures of 1.2 kg/cm², 2.4 kg/cm² and 4.8 kg/cm², and in all cases include large stress reversals in the triaxial plane, $\sigma_{22} = \sigma_{33}$.

On the basis of the calibrated model, the following figures 6 through 8 show how the model response compares with the physical triaxial test data, i.e. how accurately the model reproduces the test data used to calibrate it.

The abrupt stiffness reduction occurring when a friction mechanism shifts from passive to active status appear in figure 6 at points (1p) - (4p) during primary triaxial compression, at (1u) - (2u) during reversed loading into triaxial extension, and at (1r) - (4r) during re-reversed loading into triaxial compression. Note how the model captures Bauschinger effect. Point (1u), indicating on-set of shear slip in triaxial extension in friction mechanism 1, even occurs for a compressive stress difference, σ_{11} - $\sigma_{33} > 0$. This is due to previous slip for the primary compressive loading.

Figures 6, 7 and 8 include physical data points (circles for σ_{11} - σ_{33} vs. ε_{11} and triangles for ε_{vol} vs. ε_{11}) and they all show how the model captures physically observed Bauschinger effect.

Following the large stress reversal in test SM-L9-4.8, figure 6, it is clear that the material has densified and gained strength from the large stress cycle. This explains the ~20% increase in stress difference observed after the cycle. At present the model does not include such effect of void ratio change. The model response simply approaches an imaginary primary branch which

would have been observed in the physical test, had there been no stress cycle, i.e. the broken thin line including breakpoint (4p).

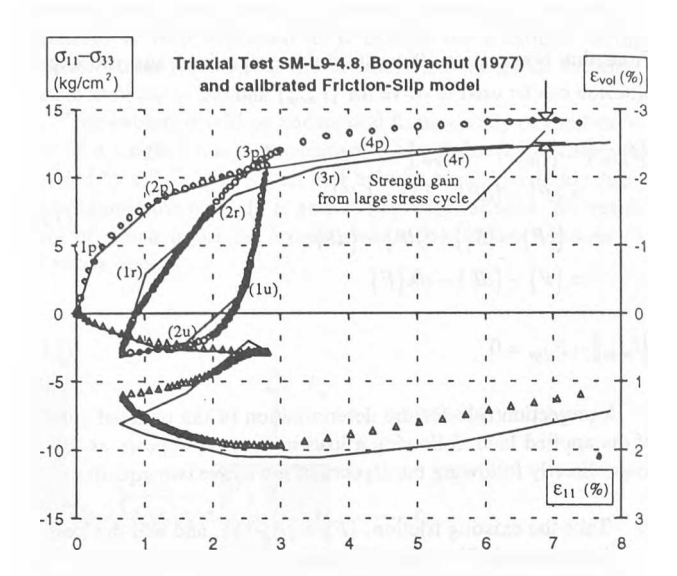


Figure 6. Calibrated model and Boonyachut (1977) triaxial test data SM-L9-4.8

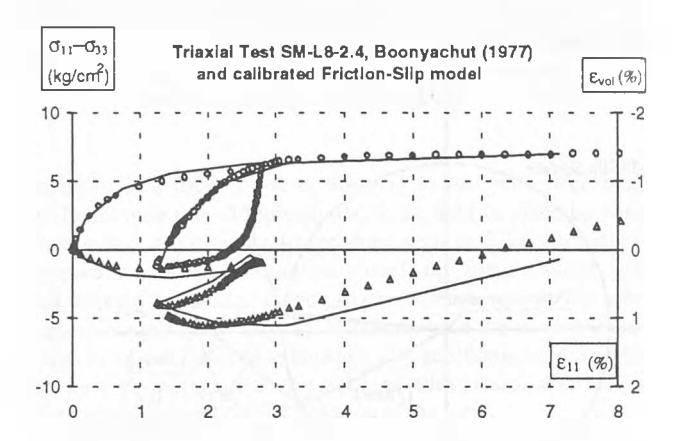


Figure 7. Calibrated model and Boonyachut (1977) triaxial test data SM-L8-2.4

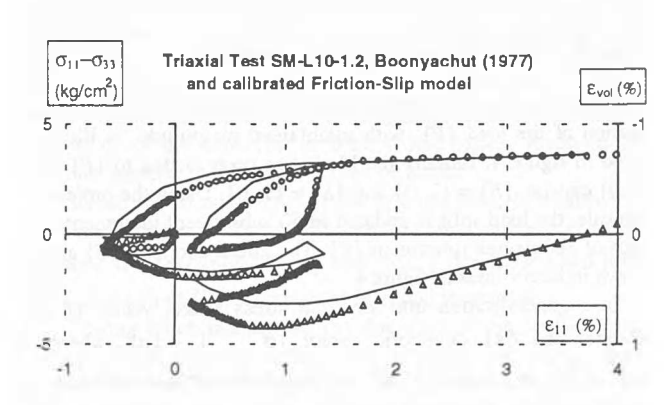


Figure 8. Calibrated model and Boonyachut (1977) triaxial test data SM-L10-1.2

5. EXTRAPOLATION TO TORSION-SHEAR DATA

The model, once calibrated to the three triaxial tests of Boonyachut (1977), was then used to predict three torsion-shear tests, originally carried out by Geiger (1979), on the same loose Santa Monica Beach sand (void ratio, e = 0.81) as used in the triaxial tests of Boonyachut. The confining pressure used in all torsion-shear tests was $\sigma_{33} = 2.0 \text{ kg/cm}^2$.

It is important to notice, that the model was not calibrated nor in any way modified - to match the torsion-shear data by Geiger.

The torsion-shear apparatus and the use of it has been thoroughly described by Lade (1981). It uses a hollow cylinder specimen, and the vertical axial load, σ_{22} , the confining pressure, $\sigma_{11} = \sigma_{33}$, and the torque, σ_{12} , can be applied individually. The orientation of stresses on the hollow cylindrical specimen is shown in figure 9.

A view of the torsion-shear apparatus is shown in fig. 10.

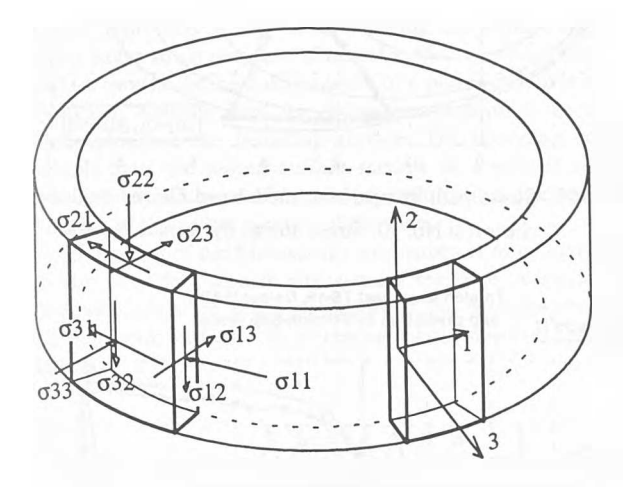


Figure 9. Stress Components in Cartesian Coordinate System for Hollow Cylinder Specimen

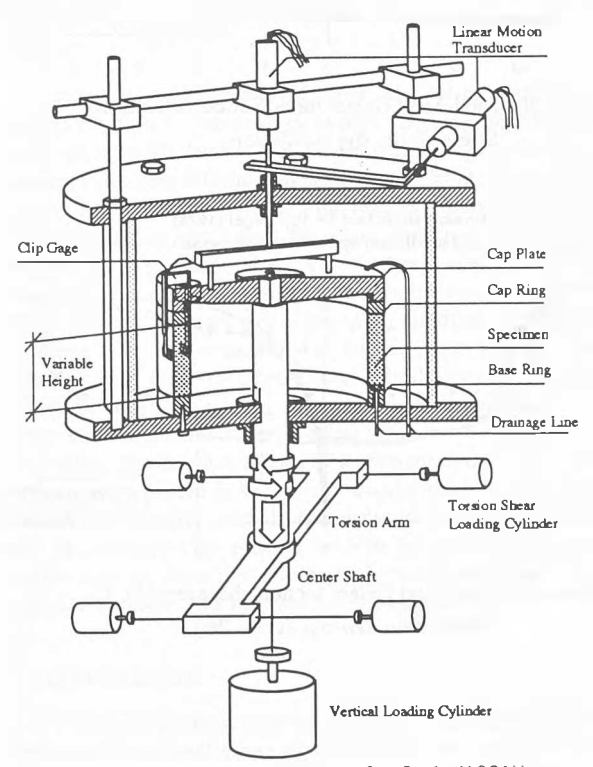


Figure 10. Torsion-shear apparatus (after Lade (1981))

The applied loading paths in Geiger's torsion-shear tests have taken their specimens well into inelastic shear behavior and often very close to failure. The strains become very sensitive to the stresses, as the stresses approach failure. For accurate portrayal of the potential of the model, it should be noted that the loading used to calculate deformations may deviate slightly from the actual load path in the test, in order to arrive at correct experimentally observed strain levels, where large inelastic straining occur. The deviations appear for each torsion-shear test from corresponding stress path diagrams, see figures 11, 15 and 19.

The four egg shaped contours shown in the stress path diagrams, figures 11, 15 and 19, represent traces of the four friction mechanism slip surfaces in the torsion-shear stress subspace of σ_{12} versus σ_{22} - σ_{33} .

All of the below diagrams, figures 11 through 22, show that the 3-D Friction-Slip model, figure 1, has the potential of capturing correctly the soil behavior as observed in the torsion-shear apparatus under complex load paths involving large stress reversals and stress field rotations. Except from sometimes overshooting, sometimes undershooting, the volumetric strain, the model very closely predicts the data.

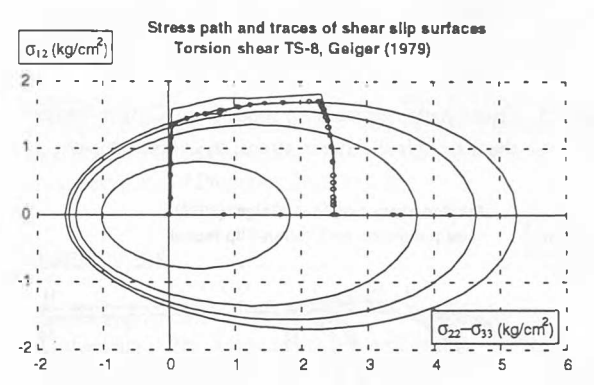


Figure 11. Stress path comparison, model and Geiger torsionshear test No. 8. Stress-stress: σ₁₂ versus σ₂₂-σ₃₃

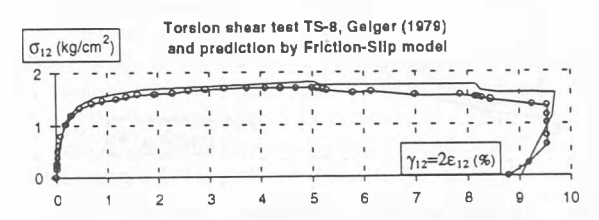


Figure 12. Model and Geiger torsion-shear test No. 8 Stress-strain: σ₁₂ versus 2ε₁₂

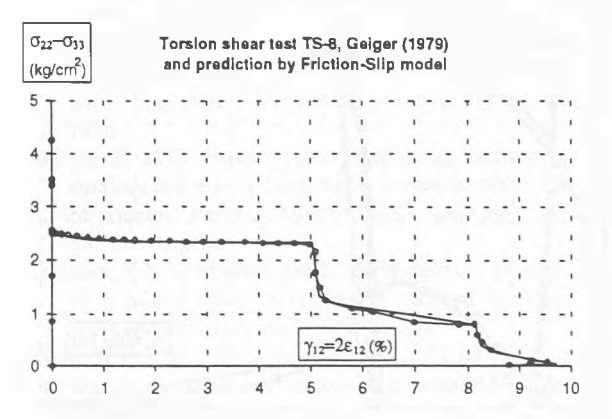


Figure 13. Model and Geiger torsion-shear test No. 8 Stress-strain: σ₂₂-σ₃₃ versus 2ε₁₂

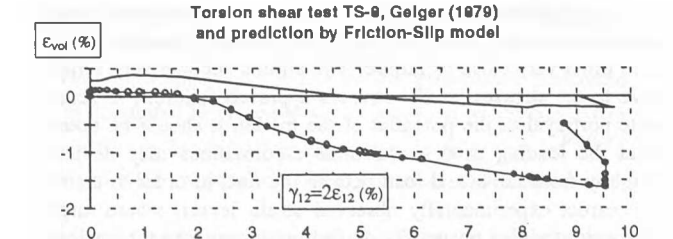


Figure 14. Model and Geiger torsion-shear test No. 8 Strain-strain: ε_{vol} versus $2\varepsilon_{12}$

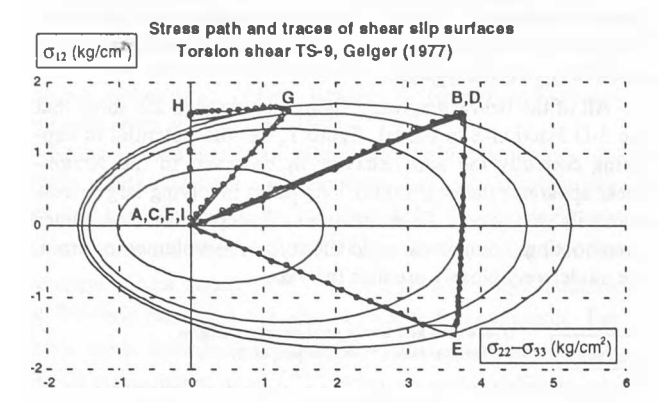
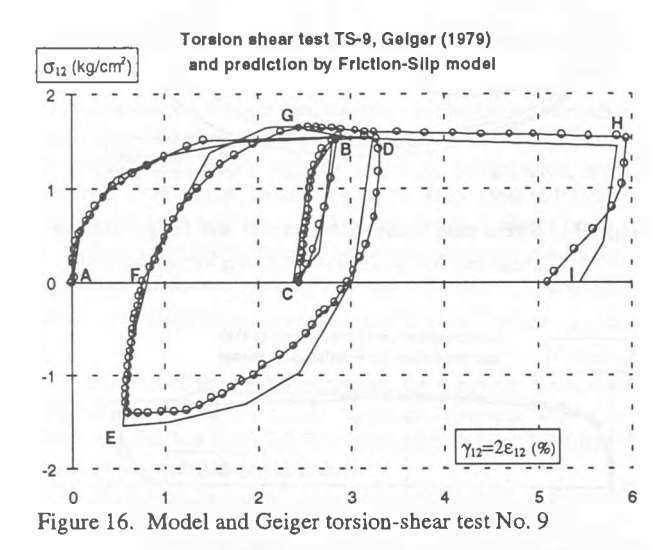


Figure 15. Stress path comparison, model and Geiger torsionshear test No. 9. Stress-stress: σ₁₂ versus σ₂₂-σ₃₃



Torsion shear test TS-9, Gelger (1979) and prediction by Friction-Silp model

E

Torsion shear test TS-9, Gelger (1979)
and prediction by Friction-Silp model

Torsion shear test TS-9, Gelger (1979)
and prediction by Friction-Silp model

Torsion shear test TS-9, Gelger (1979)
and prediction by Friction-Silp model

Figure 17. Model and Geiger torsion-shear test No. 9

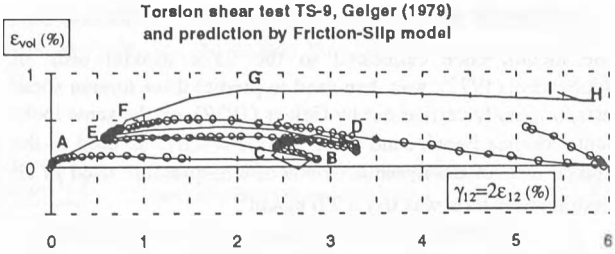


Figure 18. Model and Geiger torsion-shear test No. 9

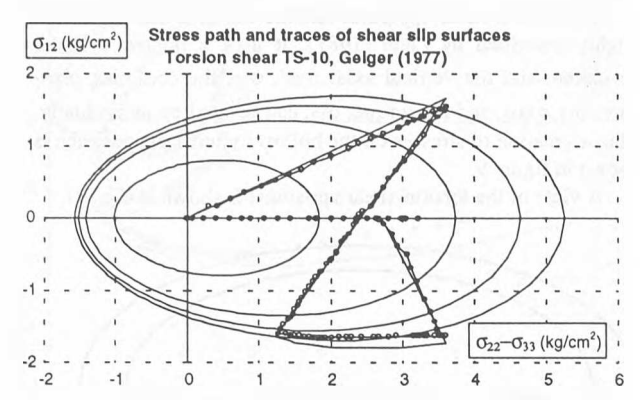


Figure 19. Stress path comparison, model and Geiger torsionshear test No. 10. Stress-stress: σ_{12} versus σ_{22} - σ_{33}

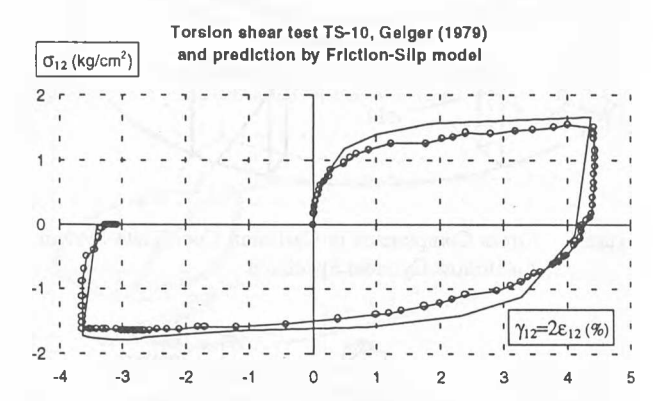


Figure 20. Model and Geiger torsion-shear test No. 10 Stress-strain: σ_{12} versus $2\epsilon_{12}$

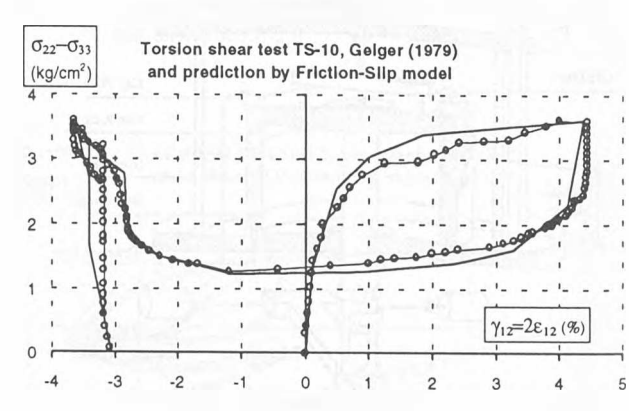


Figure 21. Model and Geiger torsion-shear test No. 10 Stress-strain: σ₂₂-σ₃₃ versus 2ε₁₂

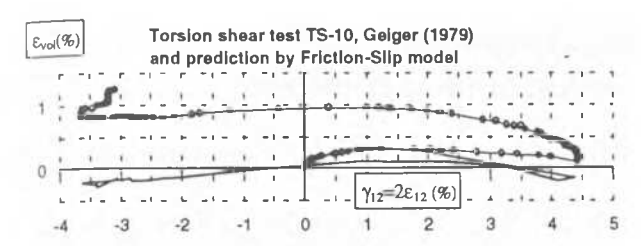


Figure 22. Model and Geiger torsion-shear test No. 10 Strain-strain: Evol versus 2E₁₂

6. FRICTION MECHANISM FOR SMOOTH RESPONSE

The abrupt stiffness change which occurs whenever a friction mechanism shifts between active and passive status may be considered a modeling disadvantage.

The bounding surface models, Dafalias (1984, 1986), Dafalias & Hermann (1982, 1986) and Anandarajah & Dafalias (1986) represents a way of overcoming the typical stepwise linear stress-strain response of nested surface models. Bounding surface models define a dependence of a plastic modulus on the Euclidean distance from the current stress point to an image stress point on the bounding surface. The bounding surface models have the nested surface models as a special case in which the dependence of the plastic modulus is a discontinuous function of the before mentioned distance.

If the idea of the friction-slip mechanism is to be carried on to also provide a smooth stress-strain response, a single continuous mechanism could be suggested (as emerged in a discussion with Professor Bent Hansen of the Danish Technical University):



Figure 23. A friction mechanism with smooth stress-strain response

Instead of the SH series of block and spring mechanisms used so far, figure 1, an analogy using a single spring resting by itself on a rough base could be imagined, figure 23. Here, loading will cause deformation of the spring from the left end in figure 23, gradually transferring the load as friction to the base. The more loading, the longer the active portion of the spring is, and the softer the response is. The right end of the spring carries no load until the capacity of the mechanism is completely exhausted. For arbitrary cyclic loading a distribution of friction along the base will occur, equal to the derivative of the internal distribution of the spring load. Generalised to stress space, the distribution of friction along the spring base becomes a density distribution of friction stress in stress space.

Rather than keeping record of a discrete number of friction stress tensors, record is kept of the density distribution of all 6 friction stress components. In this way, the Friction-Slip model can be developed to provide smooth stress-strain response, maintaining the attractive interpretable mechanical basis of the model. At present, this idea has not been pursued.

7. CONCLUSIONS

A time independent constitutive model for the elasto-plastic response of frictional materials to arbitrary load paths has been developed. The model makes use of detailed 'sublayer information' as originally suggested by the inventors of nested surface modeling theory.

The model successfully extrapolates stress-strain behavior from conventional triaxial laboratory tests to stress-strain behavior for complex torsion-shear stress paths involving large stress reversals and back and forth stress field rotation.

The model has further been developed as an ABAQUS compatible user defined material subroutine, UMAT. The subroutine makes use of 'compatibility iterations' to iterate on the stress increment, in order for the calculated strain increment to match the ABAQUS supplied strain increment. All of the diagrams shown above have been verified running ABAQUS with the UMAT subroutine.

Finally, a development of the friction-slip mechanism is proposed according to which the model can be developed to provide smooth stress-strain relations, and still maintain the attractive mechanical analogy which governs the model behavior

ACKNOWLEDGEMENTS

The theoretical research presented here has taken advantage of existing physical test data publicly available from the UCLA libraries. The important value of the Santa Monica Beach sand data set formed through the extensive laboratory work of Boonyachut (1977), Geiger (1979), and Prabucki & Lade (1990) is certainly acknowledged. All of this laboratory work was carried out in the UCLA soil mechanics laboratory under the supervision of Professor Poul V. Lade.

REFERENCES

Anandarajah, A.M. & Dafalias, Y.F., 1986: Bounding surface plasticity. III: Application to anisotropic cohesive soil, ASCE Journal of Engineering Mechanics, Vol. 112, No. 12, December 1986

Arthur, J.R.F., Chua, K.S., Dunstan, T. & Rodriguez del C., J.I., 1980: Principal stress rotation: A missing parameter, ASCE Journal of the Geotechnical Engineering Division, Vol. 106, No. GT4

Boonyachut, S. & Lade, P.V., 1977: Experimental study of the behavior of cohesionless soil during stress reversals. Report to the National Science Foundation, *University of Califor*nia Los Angeles Engineering Report, UCLA-ENG-7710

Christensen, C.T., 1995: A constitutive model for frictional materials subjected to arbitrary stress or strain paths. *Ph.D. Dissertation*, University of California, Los Angeles

Dafalias, Y.F., 1986: Bounding surface plasticity. I: Mathematical foundation and hypoplasticity, ASCE Journal of Engineering Mechanics, Vol. 112, No. 9, September 1986

Dafalias, Y.F. & Hermann, L.R., 1986: Bounding surface plasticity. II: Application to isotropic cohesive soil, ASCE Journal of Engineering Mechanics, Vol. 112, No. 12, December 1986

Geiger, E, 1979: Experimental study of the behavior of cohesionless soil during large stress reversals and reorientation of principal stresses, *Master Thesis*, University of California, Los Angeles

Ishihara, K & Towhata, I, 1983: Sand response to cyclic rotation of principal stress directions as induced by wave loads, Soils and Foundations, Vol. 23, No. 4

Iwan, W.D., 1967: On a class of models for the yielding behavior of continuous and composite systems, ASME Journal of Applied Mechanics, pp 612-617

Lade, P.V., 1981: Torsion shear apparatus for soil testing,

- Geotechnical Testing Journal, GTJODJ, Vol. 1, No. 2, pp 93-101
- Mróz, Z., 1967: On the description of anisotropic workhardening, J. Mech. Phys. Solids, Vol. 15, pp. 163-175
- Mróz, Z., Norris, V.A. & Zienkiewicz, O.C., 1978: An anisotropic hardening model for soils and its application to cyclic loading, International Journal of Numerical and Analytical Methods in Geomechanics, Vol. 2, pp. 203-221
- Mróz, Z., Norris, V.A. & Zienkiewicz, O.C., 1979: Application of an anisotropic hardening model in the analysis of elastoplastic deformation of soils, Geotechnique 29, No. 1, pp. 1-34
- Mróz, Z., Norris, V.A. & Zienkiewicz, O.C., 1981: An anisotropic, critical state model for soils subjected to cyclic loading, Geotechnique 31, No. 4, pp. 451-469
- Mróz, Z. & Norris, V.A., 1982: Elastoplastic and viscoplastic constitutive models for soils with application to cyclic loading, Soil Mechanics - Transient and Cyclic Loading, Editors Pande, G.N. & Zienkiewicz, O.C., John Wiley & Sons, pp. 173-217
- Mróz, Z. & Pietruszczak, S., 1983: A constitutive model for sand with anisotropic bardening rule, *International Journal* for Numerical and Analytical Methods in Geomechanics, vol. 7, pp 305-320
- Prabucki, M.-J. & Lade, P. V., 1990: Triaxial compression tests on Santa Monica Beach sand - I and II, *University of Cali*fornia Los Angeles Engineering Report, UCLA-ENG-91-03
- Pradel, D., Ishihara, K & Gutierrez, M., 1990: Yielding and flow of sand under principal stress axes rotation, Soils and Foundations, Vol. 30, No. 1, pp. 87-99
- Prévost, J.H., 1977: Mathematical modeling of monotonic and cyclic undrained clay behavior, *International Journal of Numerical and Analytical Methods in Geomechanics*, Vol. 1, pp. 195-216
- Prévost, J.H., 1978: Plasticity theory for soil stress-strain behavior, ASCE Journal of the Engineering Mechanics Division, Vol. 104, No. EM5, pp 1177-1194